Published in final edited form as:
J Mol Biol. 2014 March 20; 426(6): 1308–1321. doi:10.1016/j.jmb.2013.12.023.

Modulation of an ectodomain motif in the influenza A virus neuraminidase alters tetherin sensitivity and results in virus attenuation *in vivo*

Victor H Leyva Grado[a,&], **Rong Hai**[a], **Fiona Fernandes**[b,&], **Alan Belicha Villanueva**[a], **Carol Carter**[b], and **Mark A Yondola**[a,*]

[a]Icahn School of Medicine at Mt. Sinai, New York, NY

[b]Stony Brook University, Stony Brook, NY

SUMMARY

We previously demonstrated that ectodomain residue Asp_{286} in N2 neuraminidase (NA; Asp_{268} in N1 NA) present in budding-capable NA proteins contributes to productive NA plasma membrane transport partly by mediating escape from tetherin restriction[1]. Budding-incapable NA proteins contain a G at this position and either co-expression of HIV-1 vpu, or siRNA-mediated depletion of tetherin rescued budding capabilities in these proteins[1]. Furthermore, replacement of D_{286} with G in budding-capable NA proteins caused loss of function, preventing release of NA virus-like particles (VLPs). Here, we show that mutation of this residue specifically modulates the ability of NA to escape tetherin restriction at the plasma membrane and results in virus attenuation *in vivo*. Based on immunogold electron microscopy and co-immunoprecipitation assays, both NA_{D286}-containing and NA_{D286G}-containing proteins associated with tetherin in the ER. However, the NA_{D286G} loss-of-function mutant also associated with the host factor outside the ER and in plasma membrane-localized VLPs as visualized using immunogold electron microscopy. We conclude that the presence of aspartate at residue 286 liberates NA from tetherin-dependent restriction upon exit from the ER compartment thus preventing restriction at the plasma membrane. Underscoring the importance of these observations, knockdown of tetherin resulted in a 1–1.5 log increase in influenza virus growth. Additionally, the loss-of-function mutation conferred attenuation in a mouse model of influenza infection as evidenced by a 5-fold increase in LD_{50} and increases in either percent survival or time to death dependent on the administered dose *in vivo*.

Keywords

influenza; neuraminidase; ectodomain; budding; tetherin

*Corresponding author, Current address: Avatar Biotechnologies, AIDS Vaccine Design and Development Laboratory, Brooklyn Army Terminal, 140 58th Street, Bldg A, Suite 8J, Brooklyn, NY 11220. yondola@avatarbiotechnologies.com, Telephone: 6463818000 Fax: 7187651870.
&These authors contributed equally to the work.

Introduction

Virus release, the final stage in the life cycle of most viruses presents a paradoxical problem that is circumvented by evolutionarily diverse means. Since the infected cell bears the viral receptor, a means of avoiding re-entry into the previously infected cell must be accomplished allowing for viral spread to neighboring cells. Some paramyxoviruses, poxviruses, flaviviruses, herpesviruses, and lentiviruses are capable of direct cell-to-cell spread. In the case of influenza virus, an enzymatic activity encoded within the neuraminidase (NA) cleaves the sialic acid receptor from the infected cell[5; 6; 7; 8]. This allows for efficient release of nascent virions for subsequent infection of naive cells. Several other functions have also been attributed to the influenza virus NA. These include cleavage of tracheobronchial airway mucus to allow for improved virus penetration into the epithelial cell layer[9], enhancement of endosomal trafficking upon entry[10], and the presence of a hemadsorption site in some N2 NAs that increases the efficiency of sialic acid cleavage[11]. Additionally, a WSN NA strain-specific recruitment of plasminogen allowing for trypsin-independent HA cleavage has been demonstrated[12]. Using a virus-like particle (VLP) system, we and others previously demonstrated the ability of NA to form VLPs when expressed individually from plasmid DNA[1; 13]. Identification of this function suggested that NA could contribute to budding and/or release of influenza virus in a novel way. The determinant of this function mapped to a motif, present in certain influenza virus strains, on the underside of the NA globular head ($YPD_{286}\Phi$, N2 numbering, $YPD_{268}\Phi$, N1 numbering)[1]. Mutation of the critical aspartate residue (286 N2 or 268 N1 numbering) to either glycine or alanine *respectively*, cripples the budding capability of NA[1]. VLP studies using solely the NA also indicated a role for the budding-capable NA in avoiding or counteracting the antiviral restriction factor BST2/tetherin[1]. Watanabe *et al.* also confirmed a tetherin-dependent influenza VLP release restriction using a nearly complete constellation of influenza proteins[14]. However, they, and two other groups, did not find tetherin-mediated inhibition of authentic influenza virus growth[14; 15; 16]. In addition, infection of BST2 −/− mice with the influenza B virus resulted in a transient inhibition of viral lung titers found specifically at early time points[17]. These data are in contrast to a study published by Mangeat *et al*. demonstrating that tetherin does in fact inhibit influenza virus infection with an intensity roughly equivalent to other putative interferon-stimulated genes (ISGs)[18]. Therefore, controversy remains regarding the role of this factor in the inhibition of influenza virus growth.

BST-2/tetherin was originally identified in multiple myeloma patients as a cell surface marker on terminally differentiated B-cells[19; 20]. Subsequent studies identified BST-2/tetherin as an up-regulated cell surface marker on plasmacytoid dendritic cells following either influenza infection or treatment with interferon[21; 22]. It was later found that BST-2 is capable of inhibiting the release of HIV virions through formation of a protease-sensitive "tether" connecting virions to the cell surface[23; 24; 25]. These findings have been extended to numerous virus families demonstrating the broad inhibitory activity of this innate immune response[26; 27; 28; 29; 30]. Underscoring the functional relevance of these findings, many viral proteins have been identified that antagonize tetherin[23; 24; 26; 27; 31; 32]. The HIV-1 accessory protein vpu, the first viral factor found to possess this function, is able to mediate down-regulation of tetherin from the cell surface and in several cases was shown to cause the degradation of tetherin[25; 33; 34; 35; 36]. A complex glycosylation pattern causes tetherin to migrate on SDS-polyacrylamide gels as a smear between 28–40 kDa. In our experience, small differences in the appearance of the smear can be found dependent on the cell type used, demonstrating the heterogeneity of the modifications. Since these glycan modifications are added and accumulate as the protein transits from the ER through the secretory pathway, they can be used as a surrogate marker for the maturation state of the protein[24; 37]. Tetherin contains an N-terminal transmembrane domain and a C-terminal GPI

anchor. Once at the plasma membrane it localizes to lipid rafts and incorporates into both viral and cellular membranes during budding[24; 38; 39]. While the precise size of the tetherin ectodomain tolerates considerable perturbation without functional disruption, recent progress has identified this region as being critical to its antiviral activity[2; 40; 41]. Hammonds et al. found that mutation of residues within the coiled coil region of the tetherin ectodomain prevented tetherin-dependent release restriction and altered its plasma membrane localization[41]. Recent findings also suggest that plasma membrane trafficking, endocytosis, and recycling of tetherin are dependent on the small GTPase dynamin2[2; 3; 4]. It is speculated that these elements enable the protein to reach, and maintain itself in, lipid raft-enriched regions at the cell surface.

In order to further explore the functional relevance of the YPD motif present in budding-capable NA proteins, we determined the intracellular and cell surface phenotypes of gain- and loss-of-function NA mutants in this region. These studies took advantage of three closely related (greater than 90% sequence identity) N2 subtype neuraminidases that either contained (Japan/57) or lacked (Udorn/72 and Hong Kong/68) the critical YPD_{286} motif. We initially sought to determine the extent of colocalization of the various NA proteins and tetherin by immunogold thin section EM studies. This analysis demonstrated modulations in NA-tetherin colocalization at the plasma membrane based on this motif and detection of gold labeled tetherin protein specifically within release-restricted, NA(G_{286}-containing) VLPs. These findings were further supported by immunoprecipitation studies using WT NA proteins and the gain-of-function mutant Hong Kong/68 NA_{G286D}. These experiments demonstrated that while NA_{D286} associated specifically with ER-associated tetherin species, NA_{G286} associated with both ER-associated and mature forms of tetherin. We previously found that mutation of the equivalent residue D_{268} in the N1 WSN/33 strain also crippled its budding capability. We therefore utilized the WSN virus rescue system to demonstrate that loss-of-function mutation of the YPD motif results in *in vivo* virus attenuation in a mouse model of infection. Specifically, we identified a 5-fold increase in LD_{50} upon loss of function mutation and increases in either percent survival or time to death dependent on the administered dose *in vivo*. This observation underscores the relevance of this newly identified NA function in the life cycle of influenza virus.

Results

Intracellular evasion of tetherin requires NA residue D286

Since we observed that blocking tetherin restriction by siRNA-mediated depletion permits cell-surface delivery of a budding-incompetent Hong Kong/68 NA that is nevertheless capable of assembling VLPs[1], we hypothesized that NA residue 286 might specifically impact tetherin sensitivity either in transit to, or once present at the plasma membrane. To examine this possibility, we first determined, by indirect immunogold labeling at high resolution, the distribution in COS-1 cells of endogenous tetherin and NA VLPs produced by expression of Japan/57 WT NA. Prior to conducting the thin section EM experiments, we individually performed secondary only and primary/secondary antibody titrations on untransfected cells to identify antibody dilutions resulting in only minimal background staining (data not shown). Cells were then transfected with DNA encoding Japan/57 NA (D286-containing), fixed and prepared for thin-section immunoelectron microscopy. Utilization of both anti-tetherin primary and 18nm gold-conjugated secondary antibodies revealed significant labeling of tetherin at and near the plasma membrane (Figure 1A, *arrows*). However, VLPs at the cell surface, although scarce presumably due to their efficient release[1], contained no detectable tetherin (*panel 1B and inset B1*), consistent with the notion that they escape tetherin restriction. The presence of Japan/57 NA within these VLP structures was confirmed by immunogold labeling using anti-NA primary antibodies

and 12nm gold-conjugated secondary antibodies (*panel 1C*). 18 nm gold-conjugated secondary antibodies were used for NA detection in *panel 1D*.

To explore this phenomenon further, we conducted a "loss-of-function" test to determine whether the substitution of glycine for aspartate at residue 286 would cause Japan/57 NA to co-localize with tetherin. As shown in FIGURE 2A, under low power magnification, an increase in cell-associated VLPs were detected upon expression of the Japan/57 NA_{D286G} mutant. Additionally, and unlike the WT Japan/57 NA VLPs, tetherin was extensively associated with these structures (Figure 2, *insets A1 and A2*). In order to further characterize this observation, we performed NA and tetherin immunogold labeling concurrently utilizing 12nm gold conjugated beads for NA detection and 18nm gold conjugated beads for tetherin detection. As demonstrated in Figure 2, panels B and C, we frequently found NA and tetherin localized within the same VLP structure on thin section EM analysis. These observations suggest that Japan/57 NA_{D286G} encountered tetherin either during its transit to, or once localized at, the plasma membrane and support the conclusion that residue 286 in the ectodomain of the protein is a determinant of tetherin sensitivity.

The NA protein encoded by the Udorn/72 strain of influenza A virus contains glycine at position 286. To determine whether the substitution of D for G would confer escape from tetherin in the context of this strain, we performed a gain-of-function test. COS-1 cells transfected with Udorn/72 NA or a gain-of-function mutant in which D was substituted for G (Udorn/72 NA_{G286D}) were prepared for immunoelectron microscopy as described above and examined for NA and endogenous tetherin. Since no releasing VLPs are formed by either the WT or gain of function mutant[1], we observed NA and tetherin colocalization intracellularly and at the plasma membrane. Given that an IgG antibody molecule consists of three, roughly equally sized arms (2 Fab, and 1 Fc fragments) and the Fab fragment has been demonstrated to be 7 nm in length[43], we established a conservative limit of 40 nm to score colocalization of tetherin and NA intracellularly (given a maximum of 20 nm for each antibody molecule in the unlikely event that it is fully extended). As shown in FIGURE 3A, Udorn/72 NA co-localized with tetherin throughout the cytoplasm (*large inclusion, and panel D*) and at the plasma membrane (*indicated by arrows in 3A and panel B*) and was typically found within 20 nm of the labeled tetherin. In contrast, NA_{G286D} and tetherin accumulated in separate spaces (*panels 3C and 3E*), typically separated by more than 200 nm. A quantitative analysis indicated that 12 nm gold-tagged Udorn/72 NA co-localized with 18 nm gold-tagged tetherin in 21 of 40 randomly selected fields from the data set (52%, n = 2). In contrast, Udorn/72 NA_{G286D} co-localized with tetherin in 7 of 44 randomly selected fields from the data set (16%, n = 2). These results support the conclusion that residue D286 in the NA ectodomain allows the protein to bypass tetherin restriction.

NA budding competence dictates the maturation state of its associated tetherin

In order to determine if tetherin and NA interact, we performed co-immunoprecipitation experiments. 293T cells were transfected with either budding-competent (YPD-containing) Japan/57 NA or budding-incompetent Hong Kong/68 NA, with and without the co-expression of tetherin (HA-tagged just upstream of the GPI anchor and previously demonstrated to be functional)[23]. As shown in FIGURE 4, *panel A*, both Japan/57 and the Hong Kong/68 WT NA proteins co-immunoprecipitated tetherin. Interestingly, however, we noted that the migration characteristics of the associated tetherin correlated to the budding-competence of the NA. Tetherin that co-immunoprecipitated with budding-competent Japan/57 NA migrated as a single band at approximately 26 kDa (panel A) or two discrete bands migrating at approximately 26 and 30 kDa that correspond to predominantly the newly-synthesized form of the protein and protein bearing immature glycosylation (as evidenced by its EndoH-dependent removal), respectively[44; 45]. The minor bands that remain after

EndoH digestion, are also present in the PNGase treated sample and therefore may represent a yet unidentified tetherin modification. In contrast, tetherin that co-immunoprecipitated with budding-incompetent Hong Kong/68 NA migrated as a rather large smear between 28 and 43 kDa, corresponding to glycosylated forms of tetherin[37]. To further define the smear, we performed glycosidase digestion with PNGase and EndoH glycosidases. PNGase nonspecifically removes all N-linked glycans while EndoH removes only the high mannose glycans added in the ER[44; 45; 46]. Therefore, the unique specificities of the Endo H and PNGase enzymes can be used to monitor protein trafficking. Since N-linked glycosylation occurs in the ER, proteins in this organelle are sensitive to Endo H digestion. If they have entered the Golgi, where additional modifications occur to the glycan, they are resistant to Endo H digestion. As is apparent in panel 4B, treatment with PNGase or EndoH altered the migration of the NA-associated tetherin species. For both the Japan/57 NA- and the Hong Kong/68 NA–associated species, the PNGase treatment resulted in faster migrating species. In contrast to the identical effects of PNGase treatment on both samples, a significantly larger portion of the tetherin-associated with the budding incapable Hong Kong/68 NA was EndoH-resistant and therefore represented mature tetherin that had been transported out of the ER. To confirm consistency with the thin section EM results obtained in Cos-1 cells, we also performed the immunoprecipitation experiment with Hong Kong/68 NA and the gain-of-function mutant (Hong Kong/68 NA_{G286D}) in Cos-1 cells. As evident in panel 4C, the gain-of-function mutation in the Hong Kong/68 NA resulted in a phenotype that mirrored that of the budding-capable Japan/57 NA, *i.e*., loss of the slowly migrating, EndoH-resistant, species representing the post-ER forms of tetherin. Since tetherin functions at the plasma membrane and only the budding-incompetent Hong Kong/68 WT NA associates with post-ER, mature tetherin, we conclude that budding-competent NA possesses a YPD-dependent means of avoiding tetherin association after its maturation.

Tetherin is induced upon WT influenza virus infection

Tetherin is not uniformly expressed constitutively in epithelial cell lines[23; 47]. Rather, it is interferon inducible and mediates its antiviral effects following induction[21; 22; 24; 32]. Winkler et al. recently reported interferon dependent induction of tetherin upon influenza virus infection[16]. To determine whether influenza virus infection induces tetherin in our system, A549 cells were infected at an MOI of 0.05 with WT influenza A virus from both the H1N1 and H3N2 subtypes. Significant increases in tetherin expression were observed at both the mRNA and protein levels at 24 and 48 hours post infection, *respectively* (FIGURE 5). These data demonstrate that tetherin is induced upon infection with WT influenza viruses of both currently circulating human influenza virus subtypes and are in agreement with the previously published results of Winkler et al[16].

Trypsin, added exogenously to the influenza virus growth medium, results in the degradation of tetherin

The influenza virus hemagglutinin is expressed as a precursor (HA^0) that normally gets cleaved by host proteases (either trypsin or furin-like, depending on the presence of a polybasic cleavage site) during *in vivo* infection[48; 49; 50; 51]. In order to allow multi-cycle growth of influenza virus in tissue culture, TPCK-treated Trypsin is typically added to the virus growth medium allowing for cleavage of the HA^0 precursor protein into its fusion-competent form containing the HA1 and HA2 cleavage products[52]. In addition, virus growth medium is typically devoid of serum since components in serum can inhibit the activity of trypsin and impact influenza virus entry[52; 53; 54; 55]. We determined that when influenza virus was grown in standard virus growth medium (1× Minimal Essential Medium MEM supplemented with 1× P/S, 0.15% Sodium Bicarbonate, L-glutamine, 200 mM Hepes (7.4), 0.3% BSA, and 1 ug/mL TPCK-Trypsin), tetherin was rapidly degraded in the absence of any serum inhibitors of trypsin activity. This degradation was observed as early as 3 hours

post addition of virus growth medium (Figure 6A, left). These results are similar to those obtained by Hammonds et al., who demonstrated that trypsin can interfere with the inhibitory role of tetherin on HIV release[56]. To eliminate trypsin-dependent degradation in our experiments, virus growth medium containing a decreased trypsin concentration (0.5 ug/mL) and minimal amounts of serum (0.5%) was used, thus preventing its degradation and permitting multicycle replication (Figure 6A, right).

Significant controversy exists as to whether tetherin is able to exert an antiviral effect on influenza virus. Three studies demonstrated minimal or no effect on virus replication[14; 15; 16] while a study by Mangeat *et al*. demonstrated an approximately 10- to 50- fold tetherin-dependent reduction in virus titer[18]. In order to determine the functional consequences of tetherin expression on influenza virus infection in our system, we analyzed virus growth in the presence or absence of endogenously expressed tetherin. Influenza virus replicates poorly in HeLa cells which express high levels of tetherin constitutively[32]. In order to explore the contribution of tetherin to this restriction, we used lentiviral transduction to generate a polyclonal cell line that constitutively expresses an shRNA against tetherin and an additional polyclonal cell line expressing a scrambled control shRNA. The specificity of this shRNA for tetherin was confirmed in our previous study using an engineered shRNA resistant tetherin protein[1]. The lentiviral system we used (pLVX-shRNA1; Clontech) allowed enrichment of GFP-positive cells by FACS sorting. As shown in FIGURE 6, *panel A* (*right*), the tetherin knockdown efficiency within GFP-positive cells was approximately 95%. Analysis of WT PR8 virus growth in the presence and absence of the targeted shRNA revealed that tetherin contributes to restriction of influenza A virus growth in HeLa cells. We observed a 10-fold increase in virus yield upon tetherin knockdown (*panel B*). Identical results were obtained with the WSN virus strain in these cells (*panel C*). Similar results were also obtained with the recent swine flu pandemic isolate A/California/04/09 (H1N1) (*data not shown*).

Tetherin restricts influenza A virus replication in a human respiratory epithelial cell line

In order to determine if the observed results were specific to HeLa cells, lentiviral transduction was also used to generate a polyclonal cell line stably expressing either scrambled or tetherin-targeted shRNAs in the small cell lung cancer cell line NCI-H196. This cell line was selected because it is of lung epithelial origin and tetherin has been shown previously to be a cell surface marker on these cells[47]. As shown in FIGURE 7, *panel A*, the knockdown efficiency of tetherin in the cells was greater than 95% after sorting for GFP-positive cells. As shown in *panels 7B* and *7C*, the knockdown of tetherin in these cells also resulted in a 10- to 50-fold increase in virus growth for both the PR8 and WSN influenza A virus strains at an MOI of 0.5. Increased growth in this cell population was also observed in single cycle infections following tetherin knockdown. As shown in FIGURE 8, *panel A*, a 7-fold average increase in viral titer upon tetherin knockdown was observed following WSN infection at an MOI of 1.0 with harvest at 14 hours. Taken together with the findings in HeLa cells, these results indicate that tetherin restricts the replication of both lab-adapted and recently circulating H1N1 strains.

The budding/release stage of the influenza A virus life cycle is affected by tetherin

Since tetherin-mediated inhibition of influenza A virus growth was observed during a single cycle of replication, it allowed us to investigate the stage of the influenza A virus life cycle that is restricted. In order to accomplish this, budding assays were performed in the NCI-H196 cell line using the complete WSN virus in a manner described previously[1]. As shown in Figure 8B, during single cycle replication (MOI 1.0, 14 hours post infection harvest) significant increases in virus particle production were detected in the media of the tetherin-knockdown NCI-H196 cells as evident by anti-HA^0 and anti-HA2 western blot analysis.

Concurrent analysis of whole cell extracts demonstrated that equivalent viral replication had occurred as evident by equivalent levels of HA^0 and HA2 in the infected cells. These results demonstrate that late events in the influenza virus life cycle were targeted by tetherin resulting in inhibition of virus growth. This observation supports the findings of Mangeat *et al.*[18].

Loss-of-function mutation of the YPD motif in the ectodomain of the WSN neuraminidase attenuates the virus in vivo

In order to determine the functional consequences of the YPD motif in the context of influenza A virusgrowth *in vivo*, we rescued recombinant WT and mutant (YPD_{268} to YPA_{268}) WSN influenza viruses from the same plasmid set and tested them in a well-established BALB/c mouse model of influenza A virus infection. In our initial experiments, we infected mice with equivalent amounts of WT or mutant virus (500 pfu/mouse, Figure 9A) and recorded body weight loss and survival for 14 days post infection. In these experiments, we observed *in vivo* attenuation of the mutant virus as evident by greater percent survival in the mutant virus infected group (40% mutant vs 20% WT, n=10, Figure 9A). While statistical analysis of these data did not reveal significant differences, it did reveal that given a 20% difference in survival the study was considerably statistically underpowered (18.3%) and would require more than 100 animals per group in order to achieve the appropriate 80% power-level for accurate statistical analysis. In order to address this shortcoming, we performed a second set of experiments where we increased the infectious dose to 1000 pfu/mouse and utilized a lower percent body weight cutoff for the determination of lethality. Although this increased dose was lethal in 100% of the animals tested, we observed a statistically significant difference in the time to death in the group of animals infected with the mutant virus (Figure 9B, Log-rank (Mantel-Cox) p=0.047). We also performed an experiment to determine the LD_{50} of both viruses in BALB/c mice. Consistent with a role for the YPD motif in *in vivo* pathogenesis, the LD_{50} differed significantly when the rescued WT WSN virus was compared with the YPA loss-of-function mutant (121 pfu *vs* 544 pfu, *respectively*, Figure 9C). These data demonstrate that loss of function mutation of the YPD motif within WSN NA results in virus attenuation *in vivo*. Thus, the motif is a determinant of a novel NA function that contributes to the outcome of infection.

Discussion

We demonstrate that NA contains a motif on the underside of the ectodomain that confers escape from tetherin restriction and productive release of the virus from the plasma membrane. The functional relevance of this finding is underscored by tetherin-mediated inhibition of virus growth *in vitro* and attenuation of virus replication *in vivo* following loss-of-function mutation of the motif. The level of viral inhibition observed (1 to 1.5 logs and/or mild *in vivo* attenuation) is consistent with the fact that tetherin is only one of hundreds of ISGs mediating the antiviral response[57; 58]. We previously identified a role for tetherin in the inhibition of NA-driven VLP release and showed that this was linked to the YPD motif in NA[1]. We now provided evidence for tetherin-mediated inhibition of authentic influenza virus particle release. In addition, we show that NA and tetherin interact through co-immunoprecipitation experiments that are further supported by immunogold localization in thin section EM images.

We were unable to demonstrate enhanced survival using the loss-of-function mutant in tetherin-knockout mice (C57BL/6 background). However, we generated polyclonal, murine tetherin-expressing, A549 cells in a background where the human tetherin protein had been stably knocked down. Infection of these cells at an MOI of 0.2 with the loss-of-function

YPA mutant WSN virus resulted in a 6-fold inhibition of virus growth compared to WT A549 cells. However, growth of the WT WSN virus was also inhibited, albeit to a lesser degree (2.5-fold), which complicated the interpretation. Thus, we cannot completely rule out the possibility that additional factors play a role in the observed *in vivo* attenuation.

Mangeat *et al*. provided evidence that the intrinsic enzymatic activity of NA desialylates the highly glycosylated species of tetherin[18]. Our results are consistent with this possibility in addition to suggesting that budding-competent NA proteins may also be able to trap immature tetherin species in the ER. Further experiments must be performed to test this hypothesis. Although our findings are in general agreement with Mangeat *et al*., they differ from reports published by Watanabe *et al*., Bruce *et al*., and Winkler *et al.*[14; 15; 16; 18]. Possible explanations for these differences include experimental design, cell lines used, and the presence of trypsin in the influenza virus growth medium (*c.f.* Materials and Methods and Figure 6). In addition, the levels of tetherin modulation (overexpression and/or knockdown) might have differed significantly between the different studies. Although careful positive controls were evident in the studies demonstrating the lack of an effect of tetherin on influenza A virus replication, the control viruses used may have been more sensitive to tetherin-dependent restriction. The multiplicity of infection used in the Watanabe *et al.*, Bruce *et al.*, and Winkler *et al.* studies may have resulted in the differences between our findings. All three groups performed their experiments at a relatively high MOI (MOI of 1.0)[14; 15; 16]. We examined this possibility and confirmed that, at an MOI of 1.0, little to no enhancement was observed in our HeLa cell lines (3-fold *vs* 10-fold at MOI 0.5, *data not shown*). Notwithstanding the outcome in HeLa cells, our multi-cycle replication analysis and our analysis of replication in the NCI-H196 cells enabled clear differences to be observed. The utilization of our unique virus growth medium to permit multi-cycle replication without tetherin degradation facilitated this analysis. The tetherin-mediated restriction imposed on certain WT influenza A viruses possessing a G at position 286 suggests that some level of competition naturally occurs between NA and tetherin. It will be of interest to determine the precise role of the YPD and YPG motifs in circulating influenza virus strains and the presumed advantage of conserving the latter sequence.

Materials and Methods

Cells, plasmids, and reagents

A549, HeLa, (WT and shRNA-expressing) and COS-1 cells were maintained in DMEM supplemented with 1× Pen/Strep and 10% FBS. The COS-1 cells were used for thin-section immuno-electron microscopy (EM), as their flat morphology and high ratio of cytoplasm to nucleus allows improved visualization of subcellular structures. NCI-H196 cells were purchased from ATCC. Both WT and shRNA-expressing cells were maintained in ATCC RPMI medium supplemented with 10% FBS that was not heat-inactivated and 1× Pen/Strep. The plasmid (pCAGGS) encoding the NA protein of Udorn/72 was an identical match to the published GenBank sequence; the plasmid encoding the Japan/57 NA differed at one amino acid (S367G) from the published GenBank sequence (CY045806.1). The goat anti-influenza virus Singapore/57 N2 antibody (BEI resources) was used for immunogold labeling and immunoprecipitation. Antibodies against the HA and Flag epitope tags were used for immunoblotting and were purchased from Sigma (H-9658 and F-7425, respectively). The tetherin-related antibodies used included a rabbit anti-BST-2 antibody (kindly provided by Klaus Strebel). Anti-goat 12-nm and anti-rabbit 18nm gold-conjugated secondary antibodies used for thin-section EM analysis were purchased from Electron Microscopy Sciences.

Thin sectioning and electron microscopy

Cells grown on Aclar film were fixed in 4% paraformaldehyde-0.1% electron microscopy (EM)-grade glutaraldehyde in phosphate-buffered saline (PBS), soaked in 2% osmium tetroxide, dehydrated in a graded series of ethyl alcohol solutions, and embedded in Durcupan resin. Thin sections of 80 nm were counterstained with uranyl acetate and lead citrate and viewed with an FEI Tecanal BioTwinG2 electron microscope.

Tetherin induction experiments

A549 cells (approximately 8×10^5 per well) were infected in 6-well dishes at an MOI of 0.05 with the indicated viruses. Cells were harvested at 24 and 48 hours post infection and divided into two portions for analysis of tetherin mRNA (at 24 hours) and for protein quantification (at 24 and 48 hours) by qPCR and western blot, respectively. qPCR was performed on total RNA isolated with the Qiagen RNA kit according to the manufacturer's instructions. qPCR analysis was performed using the Bio-Rad CFX96 real-time system and the CFX manager software provided with the instrument. Primers for tetherin and GAPDH were purchased from SA Biosciences as part of the qPCR kit. Protein samples were assayed for total protein content using the BCA assay (Pierce) and analyzed by western blot after the addition of 0.1% bromophenol blue.

Trypsin-dependent degradation of tetherin experiments

HeLa cells were plated in 6-well dishes (6×10^5 cells/well) in standard growth medium. At T^O cells were washed 2× with PBS and medium was changed to standard influenza virus growth medium (1× Minimal Essential Medium MEM supplemented with 1× P/S, 0.15% Sodium Bicarbonate, L-glutamine, 200 mM Hepes (7.4), 0.3% BSA, and 1 ug/mL TPCK-Trypsin). Cells were harvested at 3, 6, and 24 hours by washing 2× in cold PBS and lysing cells directly in 2× SDS Sample buffer lacking bromophenol blue and reducing agent to allow for BCA protein assay (Pierce) prior to western blot analysis. Bromophenol blue (0.01%) and DTT (25mM final concentration) were added and samples were boiled again prior to western blot analysis.

Lentiviral transduction/polyclonal knockdown cell line generation

To produce stable knockdown of tetherin in mammalian cell lines, siRNA targeted sequences in tetherin, described previously[1], and a scrambled sequence control 5'-GCCCTGTATGGATCTCGTA-3') were inserted into a predetermined hairpin structure and cloned into the shRNA-2 GFP lentiviral expression system (Clontech). Lentivirus particles were generated using lenti-*gag*/*pol* 293T cells by standard transfection methods. Prior to transduction, lentiviral particles from 6 wells of transfected lenti-GP 293T's were concentrated using the lenti-X concentrator solution (Clontech) for the transduction of one well of a 6-well dish of target cells (Hela or NCI-H196). Cells were transduced by spinoculation (1,200 × g, 2 hours) in the presence of 8 ug/mL polybrene and the inoculation medium was changed 12–14 hours post transduction. After expansion, GFP-positive cells were sorted at equivalent intensities for both the scrambled and tetherin knockdown cells. In order to ensure efficient knockdown, the brightest 20% of cells were used for analysis. Cell lines were used within one to two weeks of sorting to maintain the high knockdown efficiency.

Growth curve analysis of WT influenza A virus

Hela and NCI-H196 (WT, SCRshRNA, TETHshRNA) cell lines were washed twice with PBS and infected in triplicate at an MOI of 0.5 for 1 hour at 37°C in PBS containing 0.3% BSA, 1× Penicillin/Streptomycin (P/S) and Ca^{2+}/Mg^{2+} (0.9mM/1.05mM respectively). The inoculum was then removed, cells were washed 2× with PBS, and virus growth medium was

added (DMEM, 0.5% FBS, 0.3% BSA, 1× P/S, 0.5 μg/mL TPCK Trypsin). Cells were collected immediately post the addition of growth medium (T^0) and again at 4, 8, 12, 24, and 36 hours post infection. Virus titers at the various time points were determined by plaque assay on MDCK cells.

NA and tetherin immunoprecipitation experiments

Cell lysates were prepared from 293T or Cos cells (4.5×10^6 or 3.0×10^6 respectively) expressing NA alone or NA and HA-tagged tetherin[23]. Approximately 48 hrs (panel A), or 60 hrs (panels B and C) post transfection, cells were washed 2× with cold PBS, scraped and pelleted in 1 mL of cold PBS prior to lysis in 750uL of RIPA (50mM Tris pH8.0, 150mM NaCl, 1% Igepal CA-630 (NP-40 substitute), 0.5% deoxycholate, 0.1% SDS) buffer with 1mM dithiothreitol (DTT) and a Protease Inhibitor Mini Tablet (Roche). Following incubation for 20 min at 4°C, the lysates were clarified by centrifugation (15 min at 13,000 rpm) and pre-cleared with protein A agarose (Roche) prior to immunoprecipitation. NA was immunoprecipitated with goat anti-Singapore/57 polyclonal antibody overnight at 4°C with protein A agarose (Roche) beads added to the mixture. Beads were washed 4× with RIPA buffer prior to the addition of 2× sample buffer supplemented with 50 mM fresh DTT, boiled, and analyzed by western blot (10% Bio-Rad Criterion gel).

Mouse Studies

All animal procedures were approved by the Institutional Animal Care and Use Committee (IACUC) of the Icahn School of Medicine at Mount Sinai. BALB/c female mice were purchased from Jackson Laboratories (Bar Harbor, ME) at 8- to 12 weeks of age. After arrival, animals were housed in 48 × 25 × 16 cm polypropylene cages with filter tops to minimize intercurrent infections. Food and water were provided *ad libitum*. Mice were maintained on a 12:12 h light–dark cycle at an ambient temperature of 24 ± 1 °C. For infection, mice were anesthetized by intraperitoneal injection of a mixture of ketamine (100 mg kg^{-1}) and xylazine (5 mg kg^{-1}) and infected intranasally with 500 (Figure 9A) or 1000 (Figure 9B) plaque forming units (PFUs) of either a recombinant influenza A/WSN/1933 (H1N1) or a mutant variant of this virus (NA-YPD268 to NA-YPA268). Clinical signs of infection were monitored and body weight was recorded daily. Mice that lost more than 20%, (Figure 9A) or 30% (Figure 9B) of the initial body weight were considered dead and humanely euthanized. To calculate the mouse lethal dose 50%, we used 8 to 10 week-old mice (n=5 per group) and inoculated them intranasally with different dilutions (100, 250, 625 PFUs) of the stock virus diluted in 40 ul of sterile PBS. Mice were daily monitored for mortality, weight loss, or other signs of disease over 14 days after infection. The mLD50 values were calculated by the method of Reed and Müench[59]. Survival curves were generated and analyzed using Prism 6 software (Graphpad software).

Acknowledgments

We are grateful to Zsuzsana Varga, Matthew Evans, Nicole Bouvier, Domenico Tortorella, Florian Krammer, Ian Ouellette, and Adolfo Garcia-Sastre (Mount Sinai School of Medicine) for helpful discussions. We thank Chen Wang (Mount Sinai School of Medicine), Min H. Chen, and Susan VanHorn (Stony Brook University Central Microscopy Imaging Electron Microscopy Core facility) for technical support. We thank Patrick Hearing (Stony Brook U) for providing numerous reagents, including adenovirus Type V dl309; Klaus Strebel (LMM, NIH-NIAID) for providing tetherin-related reagents; and Domenico Tortorella (Mount Sinai School of Medicine) for anti-PDI antibody. We also thank Marco Colonna and Melissa Swiecki (Washington University School of Medicine) for performing tetherin knockout mouse experiments and David Evans (Harvard Medical School) for providing tetherin-expressing 293T cell lines. This study was supported by National Institutes of Health FellowshipT32 AI07647-06 (MY), NIH NIAID R01 AI068463 (CAC), and a Stony Brook University School of Medicine Targeted Research Opportunity award to study Influenza (CAC).

References

1. Yondola MA, Fernandes F, Belicha-Villanueva A, Uccelini M, Gao Q, Carter C, Palese P. Budding capability of the influenza virus neuraminidase can be modulated by tetherin. J Virol. 2011; 85:2480–2491. [PubMed: 21209114]
2. Lau D, Kwan W, Guatelli J. Role of the endocytic pathway in the counteraction of BST-2 by human lentiviral pathogens. J Virol. 2011; 85:9834–9846. [PubMed: 21813615]
3. Rollason R, Korolchuk V, Hamilton C, Schu P, Banting G. Clathrin-mediated endocytosis of a lipid-raft-associated protein is mediated through a dual tyrosine motif. J Cell Sci. 2007; 120:3850–3858. [PubMed: 17940069]
4. Serra-Moreno R, Zimmermann K, Stern LJ, Evans DT. Tetherin/BST-2 Antagonism by Nef Depends on a Direct Physical Interaction between Nef and Tetherin, and on Clathrin-mediated Endocytosis. PLoS Pathog. 2013; 9:e1003487. [PubMed: 23853598]
5. Compans RW, Dimmock NJ, Meier-Ewert H. Effect of antibody to neuraminidase on the maturation and hemagglutinating activity of an influenza A2 virus. J Virol. 1969; 4:528–534. [PubMed: 5823234]
6. Palese P, Compans RW. Inhibition of influenza virus replication in tissue culture by 2-deoxy-2,3-dehydro-N-trifluoroacetylneuraminic acid (FANA): mechanism of action. J Gen Virol. 1976; 33:159–163. [PubMed: 978183]
7. Palese P, Tobita K, Ueda M, Compans RW. Characterization of temperature sensitive influenza virus mutants defective in neuraminidase. Virology. 1974; 61:397–410. [PubMed: 4472498]
8. Sattentau Q. Avoiding the void: cell-to-cell spread of human viruses. Nat Rev Microbiol. 2008; 6:815–826. [PubMed: 18923409]
9. Matrosovich MN, Matrosovich TY, Gray T, Roberts NA, Klenk HD. Neuraminidase is important for the initiation of influenza virus infection in human airway epithelium. J Virol. 2004; 78:12665–12667. [PubMed: 15507653]
10. Suzuki T, Takahashi T, Guo CT, Hidari KI, Miyamoto D, Goto H, Kawaoka Y, Suzuki Y. Sialidase activity of influenza A virus in an endocytic pathway enhances viral replication. J Virol. 2005; 79:11705–11715. [PubMed: 16140748]
11. Uhlendorff J, Matrosovich T, Klenk HD, Matrosovich M. Functional significance of the hemadsorption activity of influenza virus neuraminidase and its alteration in pandemic viruses. Arch Virol. 2009; 154:945–957. [PubMed: 19458903]
12. Goto H, Kawaoka Y. A novel mechanism for the acquisition of virulence by a human influenza A virus. Proc Natl Acad Sci U S A. 1998; 95:10224–10228. [PubMed: 9707628]
13. Lai JC, Chan WW, Kien F, Nicholls JM, Peiris JS, Garcia JM. Formation of virus-like particles from human cell lines exclusively expressing Influenza neuraminidase. J Gen Virol. 2010
14. Watanabe R, Leser GP, Lamb RA. Influenza virus is not restricted by tetherin whereas influenza VLP production is restricted by tetherin. Virology. 2011; 417:50–56. [PubMed: 21621240]
15. Bruce EA, Abbink TE, Wise HM, Rollason R, Galao RP, Banting G, Neil SJ, Digard P. Release of filamentous and spherical influenza A virus is not restricted by tetherin. J Gen Virol. 2012; 93:963–969. [PubMed: 22258861]
16. Winkler M, Bertram S, Gnirss K, Nehlmeier I, Gawanbacht A, Kirchhoff F, Ehrhardt C, Ludwig S, Kiene M, Moldenhauer AS, Goedecke U, Karsten CB, Kuhl A, Pohlmann S. Influenza A virus does not encode a tetherin antagonist with Vpu-like activity and induces IFN-dependent tetherin expression in infected cells. PLoS One. 2012; 7:e43337. [PubMed: 22952667]
17. Swiecki M, Wang Y, Gilfillan S, Lenschow DJ, Colonna M. Cutting edge: paradoxical roles of BST2/tetherin in promoting type I IFN response and viral infection. J Immunol. 2012; 188:2488–2492. [PubMed: 22327075]
18. Mangeat B, Cavagliotti L, Lehmann M, Gers-Huber G, Kaur I, Thomas Y, Kaiser L, Piguet V. Influenza virus partially counteracts restriction imposed by tetherin/BST-2. J Biol Chem. 2012; 287:22015–22029. [PubMed: 22493439]
19. Goto T, Kennel SJ, Abe M, Takishita M, Kosaka M, Solomon A, Saito S. A novel membrane antigen selectively expressed on terminally differentiated human B cells. Blood. 1994; 84:1922–1930. [PubMed: 8080996]

20. Ohtomo T, Sugamata Y, Ozaki Y, Ono K, Yoshimura Y, Kawai S, Koishihara Y, Ozaki S, Kosaka M, Hirano T, Tsuchiya M. Molecular cloning and characterization of a surface antigen preferentially overexpressed on multiple myeloma cells. Biochem Biophys Res Commun. 1999; 258:583–591. [PubMed: 10329429]
21. Blasius AL, Giurisato E, Cella M, Schreiber RD, Shaw AS, Colonna M. Bone marrow stromal cell antigen 2 is a specific marker of type I IFN-producing cells in the naive mouse, but a promiscuous cell surface antigen following IFN stimulation. J Immunol. 2006; 177:3260–3265. [PubMed: 16920966]
22. Asselin-Paturel C, Brizard G, Pin JJ, Briere F, Trinchieri G. Mouse strain differences in plasmacytoid dendritic cell frequency and function revealed by a novel monoclonal antibody. J Immunol. 2003; 171:6466–6477. [PubMed: 14662846]
23. Neil SJ, Zang T, Bieniasz PD. Tetherin inhibits retrovirus release and is antagonized by HIV-1 Vpu. Nature. 2008; 451:425–430. [PubMed: 18200009]
24. Perez-Caballero D, Zang T, Ebrahimi A, McNatt MW, Gregory DA, Johnson MC, Bieniasz PD. Tetherin inhibits HIV-1 release by directly tethering virions to cells. Cell. 2009; 139:499–511. [PubMed: 19879838]
25. Van Damme N, Goff D, Katsura C, Jorgenson RL, Mitchell R, Johnson MC, Stephens EB, Guatelli J. The interferon-induced protein BST-2 restricts HIV-1 release and is downregulated from the cell surface by the viral Vpu protein. Cell Host Microbe. 2008; 3:245–252. [PubMed: 18342597]
26. Kaletsky RL, Francica JR, Agrawal-Gamse C, Bates P. Tetherin-mediated restriction of filovirus budding is antagonized by the Ebola glycoprotein. Proc Natl Acad Sci U S A. 2009; 106:2886–2891. [PubMed: 19179289]
27. Sakuma T, Noda T, Urata S, Kawaoka Y, Yasuda J. Inhibition of Lassa and Marburg virus production by tetherin. J Virol. 2009; 83:2382–2385. [PubMed: 19091864]
28. Jouvenet N, Neil SJ, Zhadina M, Zang T, Kratovac Z, Lee Y, McNatt M, Hatziioannou T, Bieniasz PD. Broad-spectrum inhibition of retroviral and filoviral particle release by tetherin. J Virol. 2009; 83:1837–1844. [PubMed: 19036818]
29. Radoshitzky SR, Dong L, Chi X, Clester JC, Retterer C, Spurgers K, Kuhn JH, Sandwick S, Ruthel G, Kota K, Boltz D, Warren T, Kranzusch PJ, Whelan SP, Bavari S. Infectious Lassa virus, but not filoviruses, is restricted by BST-2/tetherin. J Virol. 2010; 84:10569–10580. [PubMed: 20686043]
30. Weidner JM, Jiang D, Pan XB, Chang J, Block TM, Guo JT. Interferon-induced cell membrane proteins, IFITM3 and tetherin, inhibit vesicular stomatitis virus infection via distinct mechanisms. J Virol. 2010; 84:12646–12657. [PubMed: 20943977]
31. Mansouri M, Viswanathan K, Douglas JL, Hines J, Gustin J, Moses AV, Fruh K. Molecular mechanism of BST2/tetherin downregulation by K5/MIR2 of Kaposi's sarcoma-associated herpesvirus. J Virol. 2009; 83:9672–9681. [PubMed: 19605472]
32. Neil SJ, Sandrin V, Sundquist WI, Bieniasz PD. An interferon-alpha-induced tethering mechanism inhibits HIV-1 and Ebola virus particle release but is counteracted by the HIV-1 Vpu protein. Cell Host Microbe. 2007; 2:193–203. [PubMed: 18005734]
33. Douglas JL, Gustin JK, Viswanathan K, Mansouri M, Moses AV, Fruh K. The great escape: viral strategies to counter BST-2/tetherin. PLoS Pathog. 2010; 6:e1000913. [PubMed: 20485522]
34. Douglas JL, Viswanathan K, McCarroll MN, Gustin JK, Fruh K, Moses AV. Vpu directs the degradation of the human immunodeficiency virus restriction factor BST-2/Tetherin via a {beta}TrCP-dependent mechanism. J Virol. 2009; 83:7931–7947. [PubMed: 19515779]
35. Goffinet C, Allespach I, Homann S, Tervo HM, Habermann A, Rupp D, Oberbremer L, Kern C, Tibroni N, Welsch S, Krijnse-Locker J, Banting G, Krausslich HG, Fackler OT, Keppler OT. HIV-1 antagonism of CD317 is species specific and involves Vpu-mediated proteasomal degradation of the restriction factor. Cell Host Microbe. 2009; 5:285–297. [PubMed: 19286137]
36. Miyagi E, Andrew AJ, Kao S, Strebel K. Vpu enhances HIV-1 virus release in the absence of Bst-2 cell surface down-modulation and intracellular depletion. Proc Natl Acad Sci U S A. 2009; 106:2868–2873. [PubMed: 19196977]
37. Andrew AJ, Miyagi E, Strebel K. Differential effects of human immunodeficiency virus type 1 Vpu on the stability of BST-2/tetherin. J Virol. 2011; 85:2611–2619. [PubMed: 21191020]

38. Kupzig S, Korolchuk V, Rollason R, Sugden A, Wilde A, Banting G. Bst-2/HM1.24 is a raft-associated apical membrane protein with an unusual topology. Traffic. 2003; 4:694–709. [PubMed: 12956872]
39. Sakuma T, Sakurai A, Yasuda J. Dimerization of tetherin is not essential for its antiviral activity against Lassa and Marburg viruses. PLoS One. 2009; 4:e6934. [PubMed: 19742323]
40. Andrew AJ, Berndsen CE, Kao S, Strebel K. The size and conservation of a coiled-coil structure in the ectodomain of human BST-2/tetherin is dispensable for inhibition of HIV-1 virion release. J Biol Chem. 2012; 287:44278–44288. [PubMed: 23152502]
41. Hammonds J, Ding L, Chu H, Geller K, Robbins A, Wang JJ, Yi H, Spearman P. The tetherin/BST-2 coiled-coil ectodomain mediates plasma membrane microdomain localization and restriction of particle release. J Virol. 2012; 86:2259–2272. [PubMed: 22130541]
42. Damke H, Baba T, Warnock DE, Schmid SL. Induction of mutant dynamin specifically blocks endocytic coated vesicle formation. J Cell Biol. 1994; 127:915–934. [PubMed: 7962076]
43. Werner TC, Bunting JR, Cathou RE. The shape of immunoglobulin G molecules in solution. Proc Natl Acad Sci U S A. 1972; 69:795–799. [PubMed: 4502932]
44. Maley F, Trimble RB, Tarentino AL, Plummer TH Jr. Characterization of glycoproteins and their associated oligosaccharides through the use of endoglycosidases. Anal Biochem. 1989; 180:195–204. [PubMed: 2510544]
45. Robbins PW, Trimble RB, Wirth DF, Hering C, Maley F, Maley GF, Das R, Gibson BW, Royal N, Biemann K. Primary structure of the Streptomyces enzyme endo-beta-N-acetylglucosaminidase H. J Biol Chem. 1984; 259:7577–7583. [PubMed: 6429133]
46. Plummer TH Jr, Tarentino AL. Purification of the oligosaccharide-cleaving enzymes of Flavobacterium meningosepticum. Glycobiology. 1991; 1:257–263. [PubMed: 1794038]
47. Wang W, Nishioka Y, Ozaki S, Jalili A, Abe S, Kakiuchi S, Kishuku M, Minakuchi K, Matsumoto T, Sone S. HM1.24 (CD317) is a novel target against lung cancer for immunotherapy using anti-HM1.24 antibody. Cancer Immunol Immunother. 2009; 58:967–976. [PubMed: 18979097]
48. Bahgat MM, Blazejewska P, Schughart K. Inhibition of lung serine proteases in mice: a potentially new approach to control influenza infection. Virol J. 2011; 8:27. [PubMed: 21251300]
49. Bottcher E, Matrosovich T, Beyerle M, Klenk HD, Garten W, Matrosovich M. Proteolytic activation of influenza viruses by serine proteases TMPRSS2 and HAT from human airway epithelium. J Virol. 2006; 80:9896–9898. [PubMed: 16973594]
50. Hamilton BS, Whittaker GR, Daniel S. Influenza virus-mediated membrane fusion: determinants of hemagglutinin fusogenic activity and experimental approaches for assessing virus fusion. Viruses. 2012; 4:1144–1168. [PubMed: 22852045]
51. Steinhauer DA. Role of hemagglutinin cleavage for the pathogenicity of influenza virus. Virology. 1999; 258:1–20. [PubMed: 10329563]
52. Klenk HD, Rott R, Orlich M, Blodorn J. Activation of influenza A viruses by trypsin treatment. Virology. 1975; 68:426–439. [PubMed: 173078]
53. Anders EM, Hartley CA, Jackson DC. Bovine and mouse serum beta inhibitors of influenza A viruses are mannose-binding lectins. Proc Natl Acad Sci U S A. 1990; 87:4485–4489. [PubMed: 2162043]
54. Krizanova O, Rathova V. Serum inhibitors of myxoviruses. Curr Top Microbiol Immunol. 1969; 47:125–151. [PubMed: 4305308]
55. Hayakawa M. Studies on serum antitrypsin. First report; inhibition mechanism of serum against tryptic proteolysis. Tohoku J Exp Med. 1951; 53:259–267. [PubMed: 14835662]
56. Hammonds J, Wang JJ, Yi H, Spearman P. Immunoelectron microscopic evidence for Tetherin/BST2 as the physical bridge between HIV-1 virions and the plasma membrane. PLoS Pathog. 2010; 6:e1000749. [PubMed: 20140192]
57. de Veer MJ, Holko M, Frevel M, Walker E, Der S, Paranjape JM, Silverman RH, Williams BR. Functional classification of interferon-stimulated genes identified using microarrays. J Leukoc Biol. 2001; 69:912–920. [PubMed: 11404376]
58. Schoggins JW, Rice CM. Interferon-stimulated genes and their antiviral effector functions. Curr Opin Virol. 2011; 1:519–525. [PubMed: 22328912]

59. Reed LJ, Muench H. A simple method of estimating fifty percent endpoints. American Journal of Hygiene. 1938; 27:493–497.

Highlights

- The functional relevance of a YPD motif within the influenza virus NA was explored.
- Mutational analyses revealed motif-dependent sensitivity to tetherin restriction.
- Tetherin was induced upon influenza virus infection and inhibited virus growth.
- Loss of function mutation resulted in *in vivo* attenuation in a BALB/c mouse model.
- Evidence for *in vitro* and *in vivo* functional relevance of this motif is provided.

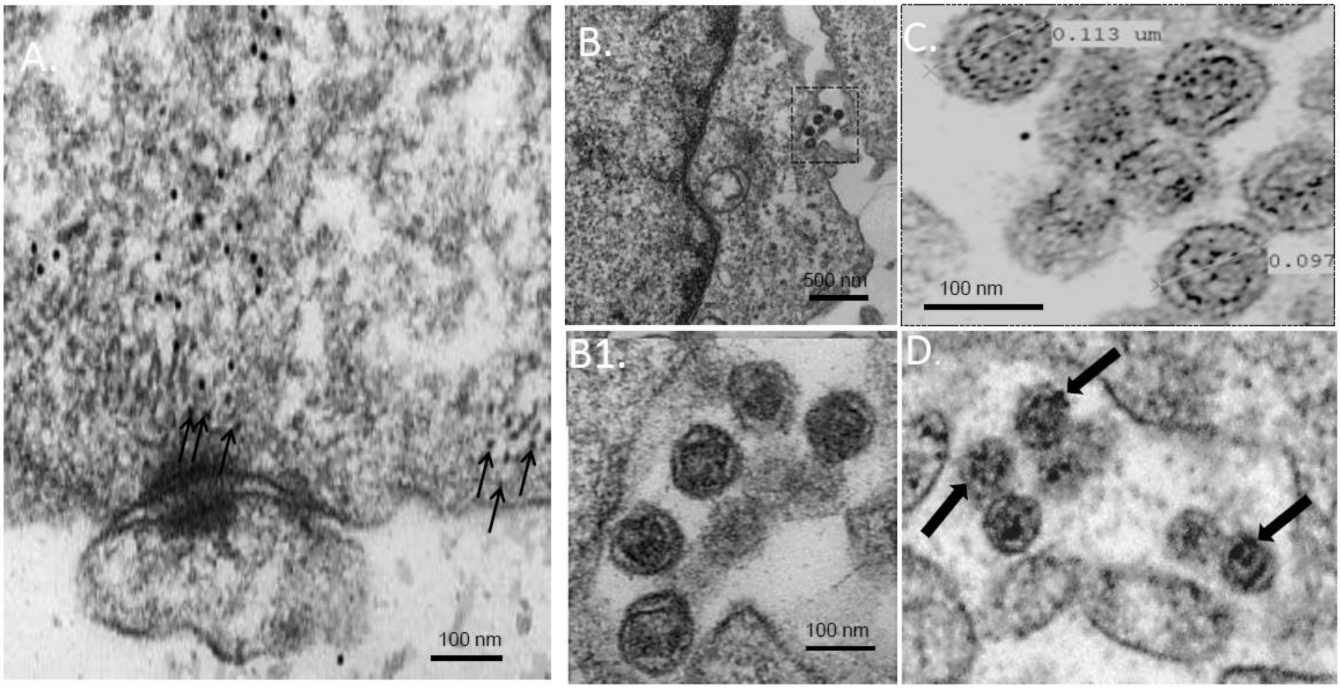

Figure 1. VLPs formed by budding-competent Japan/57 NA escape tetherin restriction at the plasma membrane

Cos-1 cells were transfected with Japan/57 NA, fixed at 48 hours post-transfection and processed for thin section immunogold labeling and electron microscopy as indicated in the Materials and Methods. Tetherin was detected with primary antibodies and labeled with secondary antibodies conjugated to 18 nm gold beads (panels A, B, and B1). NA was detected with primary antibodies and labeled with secondary antibodies conjugated to 12 nm gold beads (panel C) and 18 nm gold beads (panel D), respectively. *Panel A*, tetherin labeled at and near the plasma membrane. *Panel B and inset B1*, Japan/57 VLPs detected at the plasma membrane lacking tetherin immunogold colocalization. *Panels C and D*, Japan/57 VLPs labeled with 12 nm or 18 nm gold beads adjacent to the plasma membrane, respectively. Small arrows in panel A indicate tetherin gold labeling at and near the plasma membrane. Large arrows in panel D indicate NA gold labeling on VLPs at the cell surface.

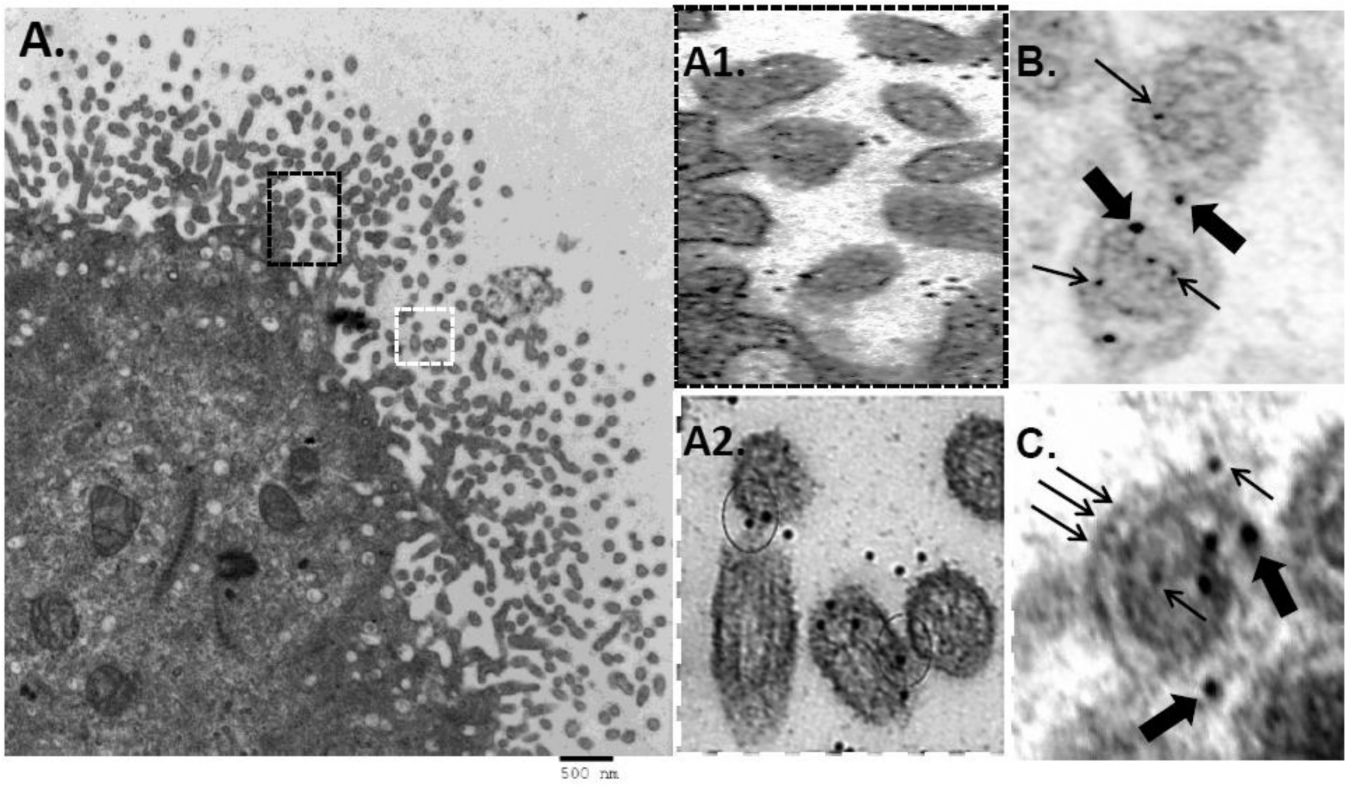

Figure 2. Loss-of-function mutation Japan/57 NA_{D286G} results in colocalization of NA and tetherin in VLPs

Cos-1 cells were transfected with the loss-of-function Japan/57 NA_{D286G} mutant, fixed at 48 hours post-transfection and processed for thin section immunogold labeling electron microscopy as described in the Materials and Methods. *Panels A-A2*, VLPs at the cell surface labeled with 18 nm tetherin gold beads; *panels B and C*, VLPs at the cell surface double labeled for NA (12nm gold) and tetherin (18nm gold). Circles in panel A2 indicate tetherin gold labeling at apparent fusion points between VLP particles. Large and small arrows in panels B and C indicate 18 nm tetherin gold labeling and 12 nm NA gold labeling within single VLPs, respectively.

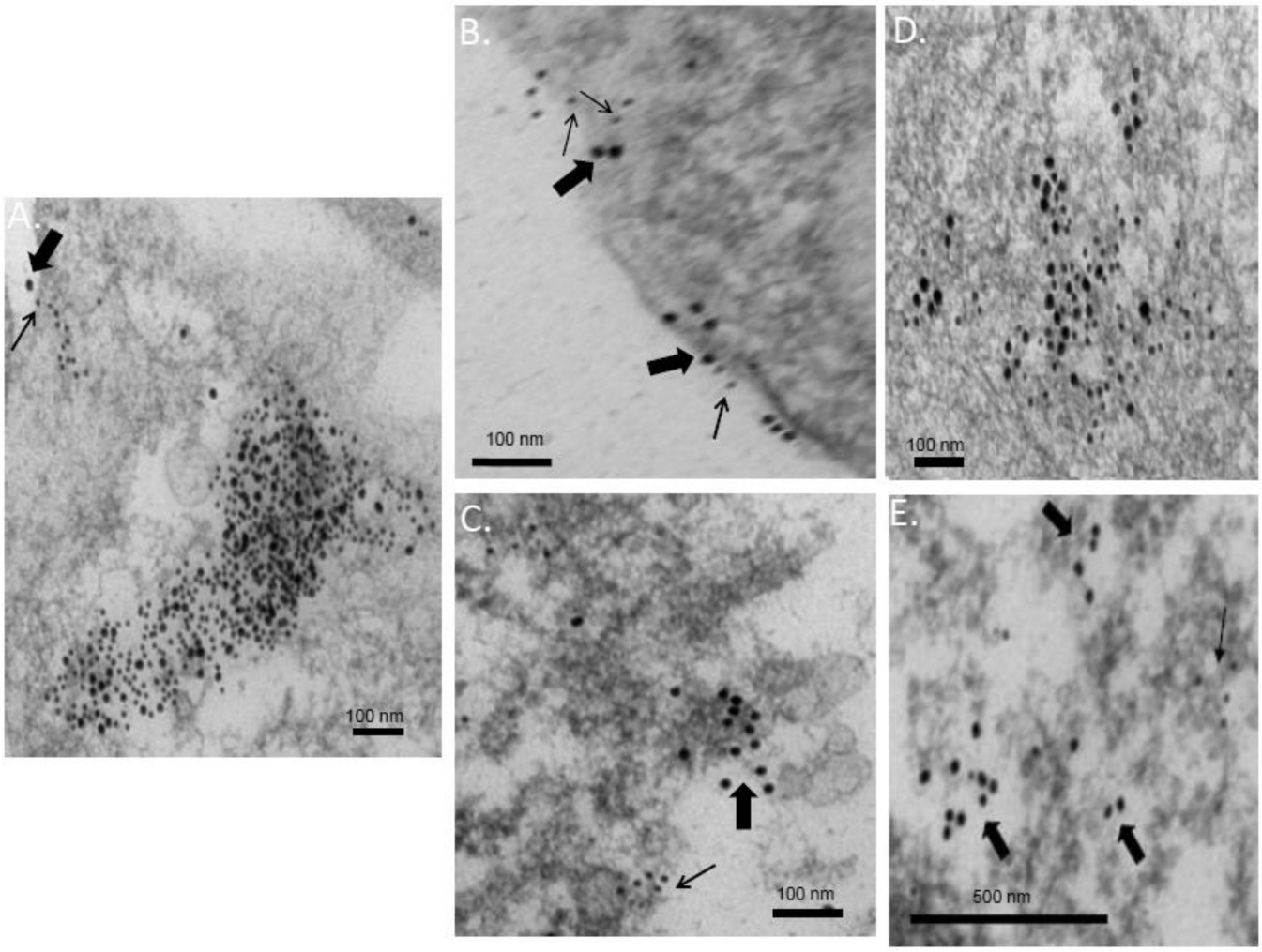

Figure 3. Gain-of-function mutation Udorn/72 NA_{G286D} rescues NA from tetherin colocalization

Cos-1 cells were transfected with either the WT or the gain-of-function Udorn/72 NA_{G286D} mutant, fixed at 48 hours post-transfection and processed for thin section immunogold labeling electron microscopy. NA and tetherin were detected with primary antibodies and labeled with secondary antibodies conjugated to 12 nm or 18 nm gold beads *respectively*. Panels *A*, B and D Udorn/72 WT NA and tetherin in the cell interior and at the plasma membrane indicated by thick (tetherin) and thin (NA) arrows. Panels C and E, Gain-of-function Udorn/72 NA_{G286D} mutant and tetherin labeling in the cell interior.

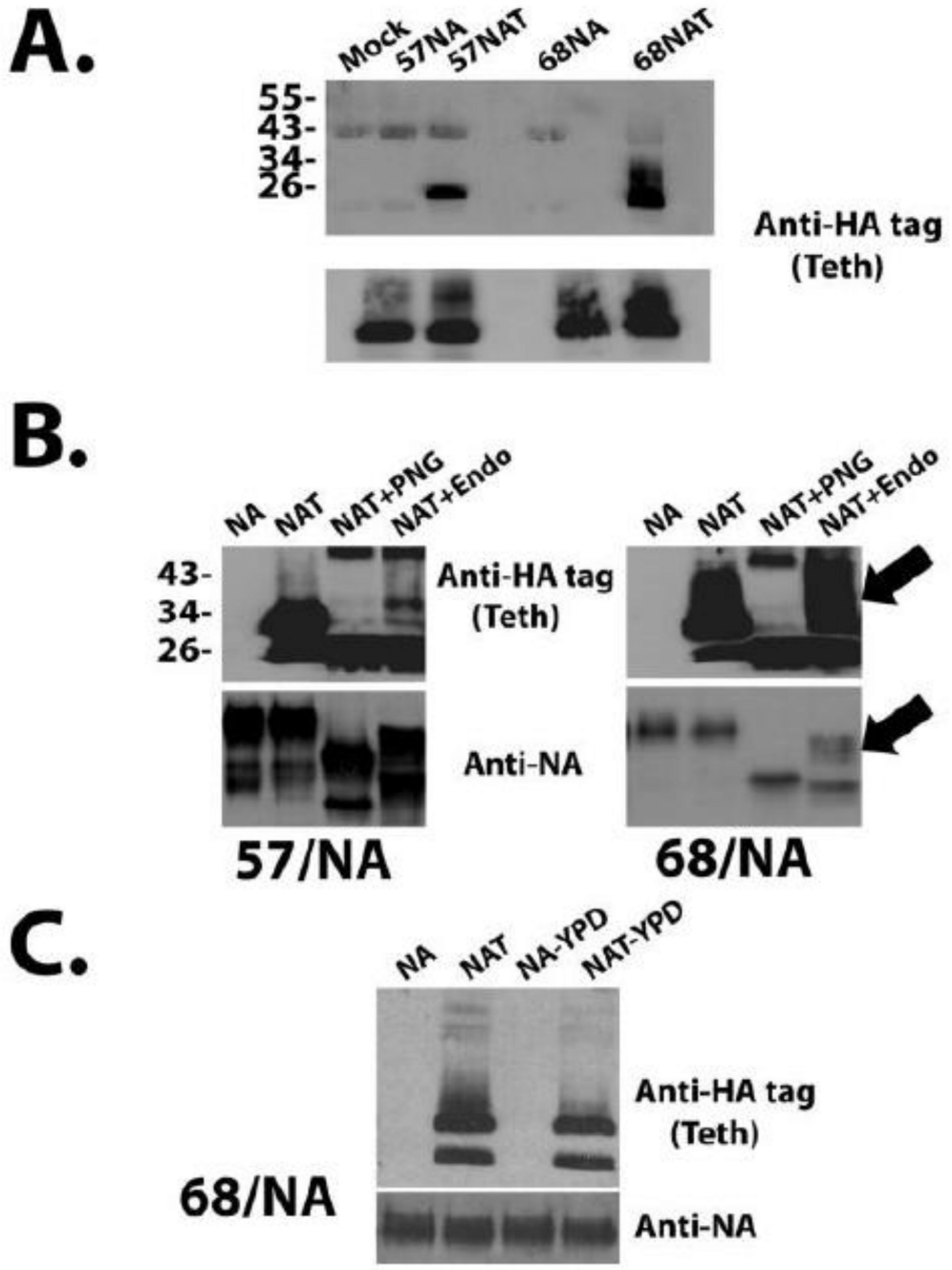

Figure 4. NA co-immunoprecipitates with tetherin and the maturation state of the bound tetherin correlates with NA budding competence

293T (*panels A and B*) or Cos-1 cells (*panel C*), were transfected with DNA encoding NA alone or co-transfected with plasmids encoding NA and tetherin, as indicated. Approximately 48–60 hours post-transfection, the cells were harvested, lysates prepared, and NA proteins immunoprecipitated. *Panel A*, NA and/or tetherin in immunoprecipitates was detected by western blotting with either anti-NA or anti-HA-tag (tetherin) antibodies. *Panel B*, Equivalent amounts of immunoprecipitated sample was either left untreated (NAT) or treated with either PNGase or EndoH prior to western blot analysis.

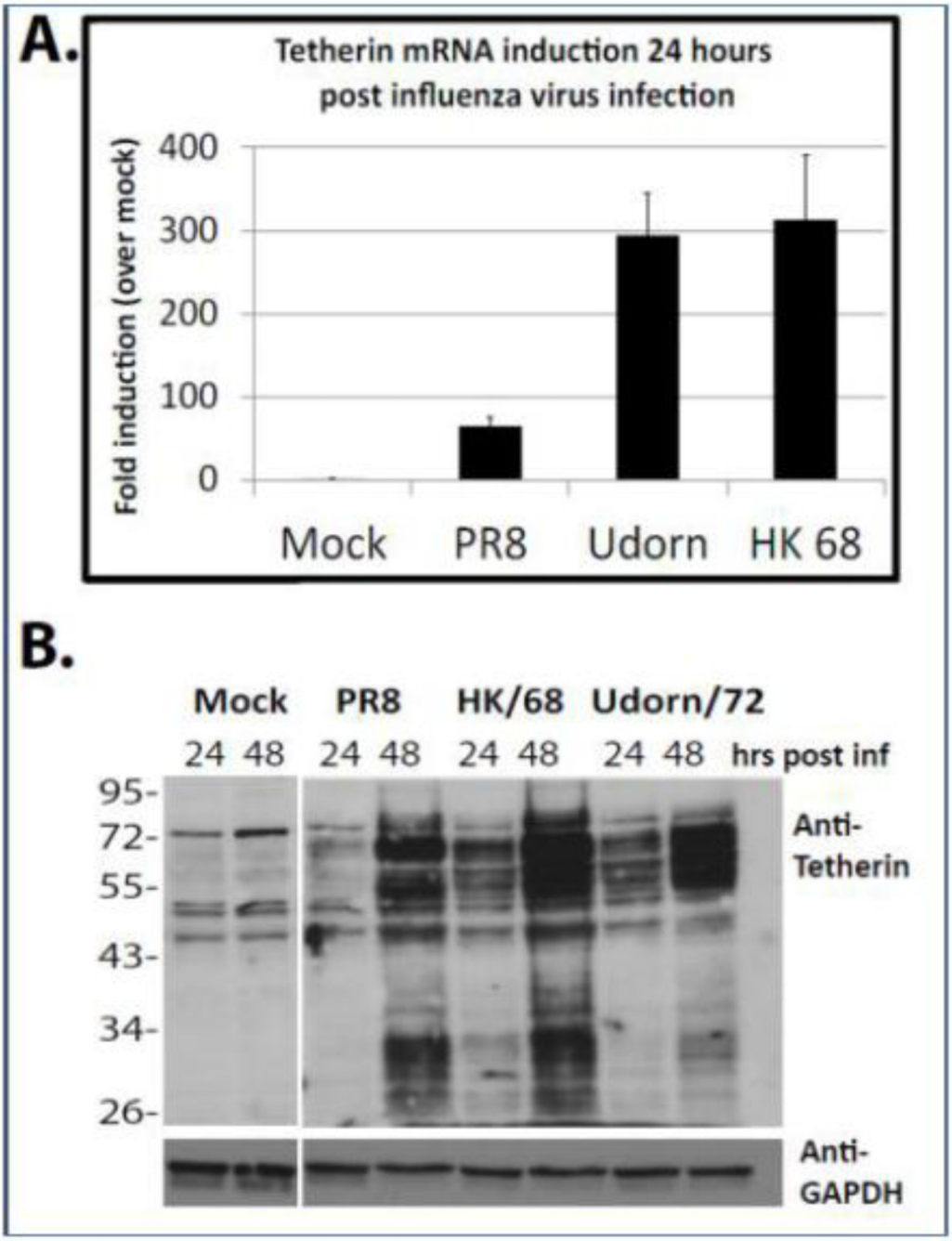

Figure 5. Tetherin is induced upon WT influenza virus infection

Panel A, A549 cells were mock-infected or infected with the indicated viruses at an MOI of 0.05. 24 hours post-infection, cells were harvested and tetherin mRNA levels were quantified by real-time PCR. *Panel B*, A549 cells were infected as in A, but were lysed directly in 2× SDS sample buffer and analyzed by western blot and non-reducing SDS-PAGE for the indicated proteins. The image shows a single western blot from which superfluous intervening lanes have been cropped.

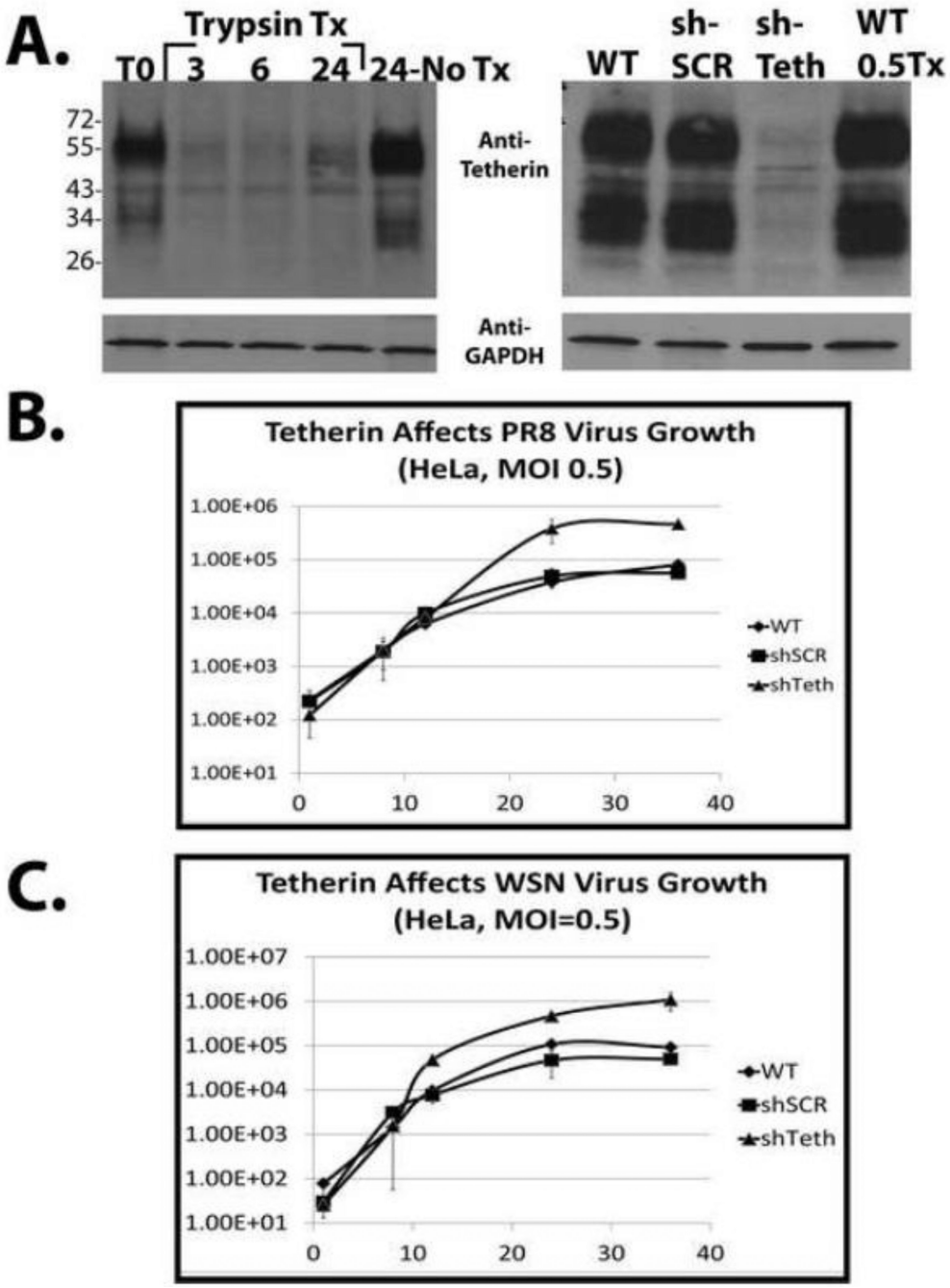

Figure 6. Tetherin contributes to the poor growth properties of influenza virus in HeLa cells

Panel A, left, HeLa cells were washed 2× and the medium was either unchanged (control), or changed to standard influenza virus growth medium (trypsin-containing) as described in the text. Just prior to the addition of virus growth medium, T^0, and at 3, 6, and 24 hours post medium change, cells were lysed and analyzed by western blot. *Panel A, right*, Cells were infected at moi = 0.05 and then incubated in the tetherin-sparing virus growth medium described in the results. 24 hours after medium transfer, the cells were lysed and the efficiency of shRNA-mediated stable tetherin knockdown was determined by western blot. Anti-Glyceraldehyde-3-phosphate dehydrogenase (GAPDH) antibody was used as a loading

control. *Panel B*, Virus growth analysis performed after infection of the indicated HeLa cell lines with either WT PR8 (*top*) or WT WSN (*bottom*) viruses at an MOI of 0.5. Virus titration was performed by standard plaque assay on MDCK cells.

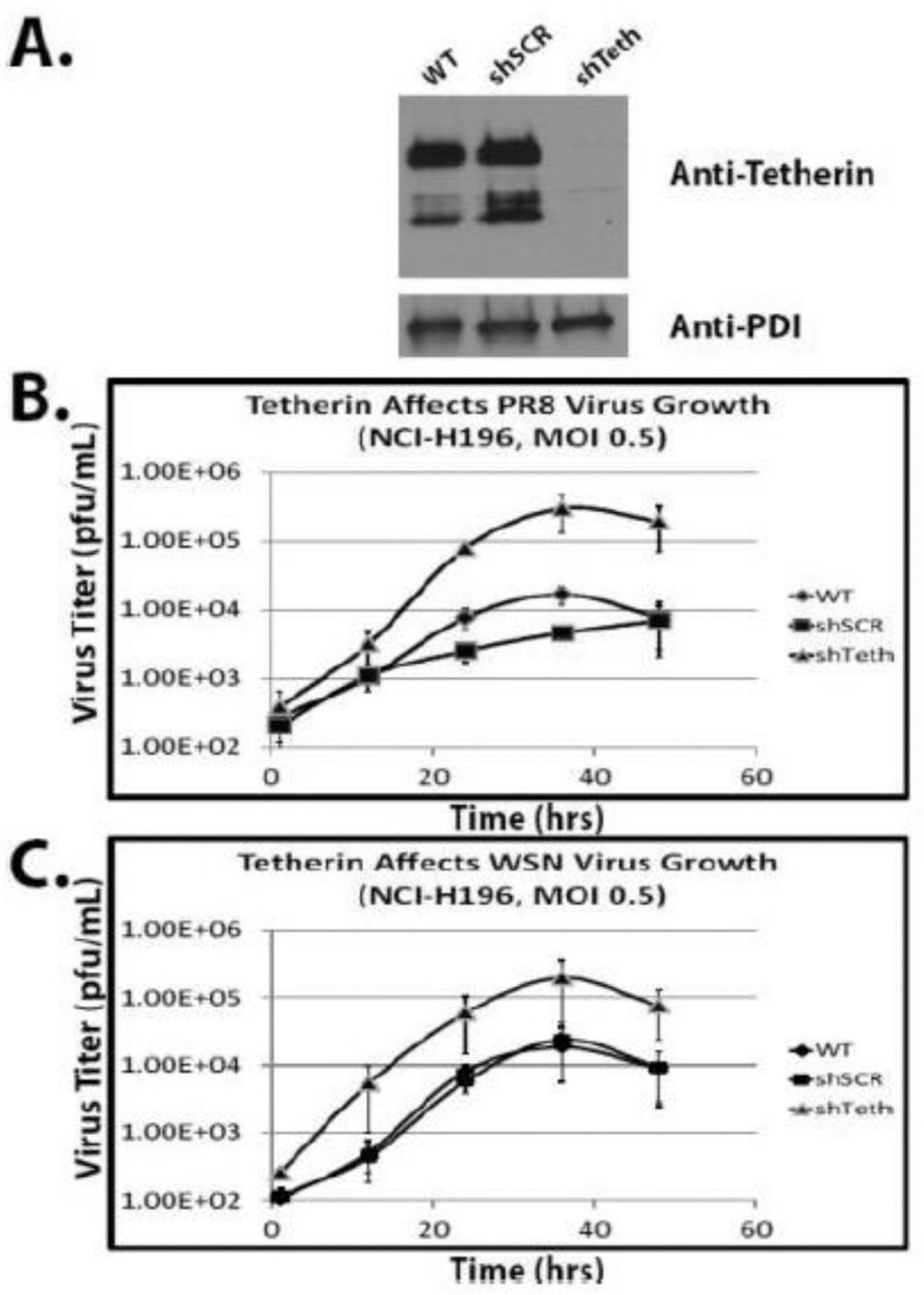

Figure 7. Tetherin inhibits influenza virus replication in the small cell lung cancer cell line NCI-H196

Panel A, At the time of infection, the indicated stable cell line was washed twice with cold PBS and lysed directly in 2× SDS sample buffer. The efficiency of shRNA-mediated tetherin knockdown was determined by western blot. Anti-protein disulphide isomerase (PDI) antibody was used as a loading control. *Panel B*, Virus growth analysis performed after infection of the cell line with either WT PR8 (*top*) or WT WSN (*bottom*) virus at an MOI of 0.5. Virus titration was performed by standard plaque assay on MDCK cells.

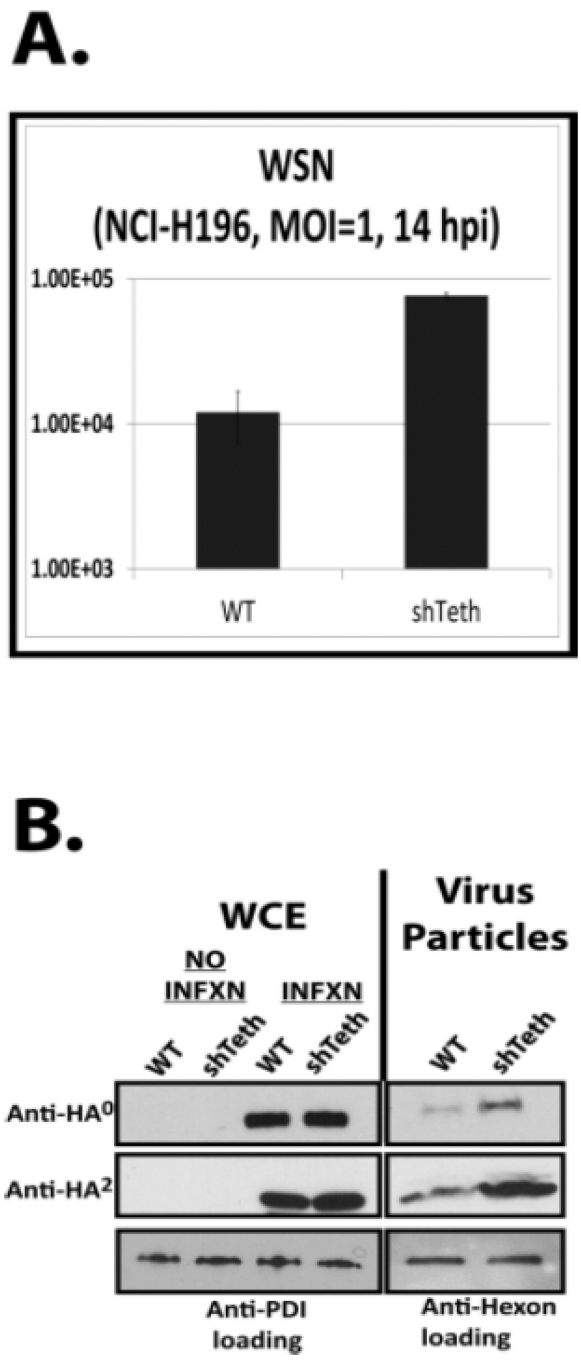

Figure 8. Late events in the influenza life cycle are specifically targeted by tetherin

WT and stable, tetherin shRNA-expressing, NCI-H196 cells were infected at an MOI of 1.0 and virus present in supernatants was quantified by plaque assay (*panel A*) or purified over a sucrose cushion for western blot analysis (*panel B*). As a loading control for tissue culture supernatants, equal amounts of WT Adenovirus (dl309) were added to each sample prior to centrifugation. Whole cell extracts were also prepared and analyzed. Anti-PDI antibody was used as a loading control for whole cell extracts (WCEs).

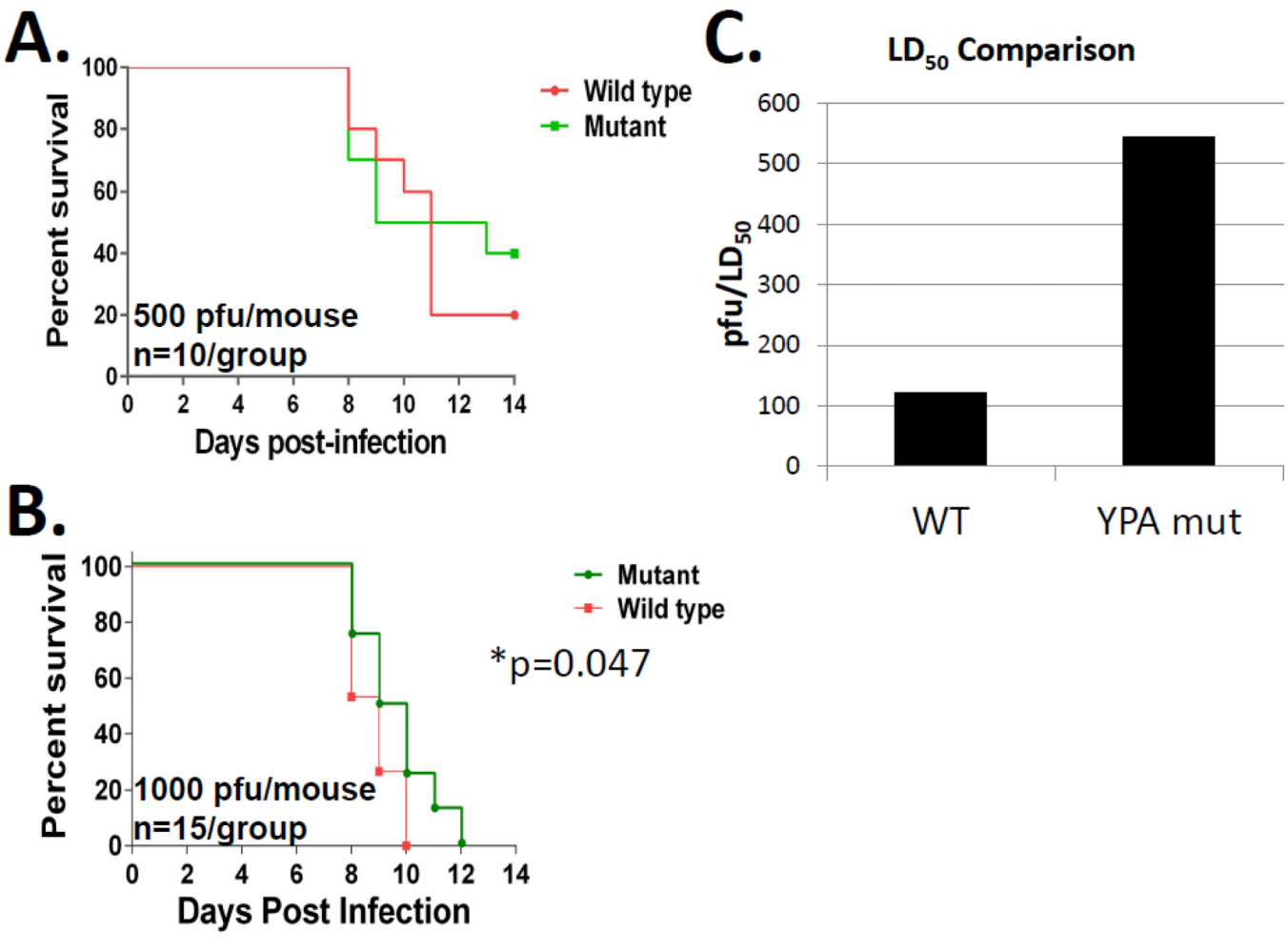

Figure 9. Mutation of the YPD motif results in virus attenuation in a BALB/c mouse model of infection

Female BALB/c mice were intranasally inoculated with 500 (*panel A*, total n=10, *2×group*) or 1000 PFUs (*panel B*, total n=15, *1×5/group and 1×10/group*) of either mutant (*Mut*) or wild type (*WT*) virus. Mice were followed for 14 (*panel A*) or 12 (*panel B*) days after infection and death was defined as a greater than 20% (*panel A*) or 30% (*panel B*) reduction in initial body weight and used to generate survival curves. The asterisk in panel B represents a statistically significant difference (Log-rank, Mantel Cox test) in time to death between the WT and mutant infected groups. *Panel C*. Mouse lethal dose 50% (LD50's). Mice were inoculated with different doses of either the wild type or the mutant viruses and followed for survival for 14 days. Mice that lost more than 25% of their initial body weight were considered dead and humanely euthanized accordingly. LD50s were calculated using the method of Reed and Muench[59]. The bar graphs represent the LD_{50} values for both the WT and mutant viruses.